Virologica Sinica 40 (2025) 236–246

Contents lists available at ScienceDirect

Virologica Sinica

journal homepage: www.keaipublishing.com/en/journals/virologica-sinica
www.virosin.org

Research Article

Structure-function insights into the dual role of African swine fever virus pB318L: A typical geranylgeranyl-diphosphate synthase and a nuclear import protein

Hai-Fan Zhao [a,b,1], Ying Wang [b,c,1], Xiao-Hong Liu [d,1], Xian-Hui Liu [e], Zhi Geng [b], Zeng-Qiang Gao [b], Li Huang [d], Chang-Jiang Weng [d], Yu-Hui Dong [b,*], Heng Zhang [b,*]

[a] School of Life Sciences, University of Science and Technology of China, Hefei 230027, China
[b] Beijing Synchrotron Radiation Facility, Institute of High Energy Physics, Chinese Academy of Sciences, Beijing 100049, China
[c] Key Laboratory of Integrated Pest Management on Crops in East China, Ministry of Agriculture, Nanjing Agricultural University, Nanjing 210095, China
[d] State Key Laboratory for Animal Disease Control and Prevention, Harbin Veterinary Research Institute, Chinese Academy of Agricultural Sciences, Harbin 150040, China
[e] College of Animal Science and National Engineering Center for Swine Breeding Industry, South China Agricultural University, Guangzhou 510642, China

ARTICLE INFO

Keywords:
African swine fever virus (ASFV)
Prenyltransferase
Geranylgeranyl-diphosphate synthase
Crystal structure
Nuclear localization signal
Immune evasion

ABSTRACT

African swine fever virus (ASFV) pB318L is an important protein for viral replication that acts as a membrane-bound *trans*-geranylgeranyl-diphosphate synthase (GGPPS) catalyzing the condensation of isopentenyl diphosphate (IPP) with allylic diphosphates. Recently we solved the crystal structure pB318L lacking N-terminal transmembrane region and performed a preliminary structural analysis. In this study, structure-based mutagenesis study and geranylgeranyl pyrophosphate (GGPP) production assay further revealed the key residues for the GGPPS activity. Structural comparison showed pB318L displays a strong similarity to typical GGPPSs instead of protein prenyltransferases. The phylogenetic analysis indicated pB318L may share a common ancestor with the GGPPSs from *Brassicaceae* plants rather than from its natural host. The subcellular localization analysis showed pB318L is localized in both nucleus and cytoplasm (including the endoplasmic reticulum membrane and mitochondria outer membrane). A unique N-terminal nuclear localization signal (NLS) following the transmembrane region was discovered in pB318L and the NLS was confirmed to be required for the nuclear import. We further revealed the NLS plays an essential role in the interaction with nuclear transporter karyopherin subunit alpha 1 (KPNA1). Their interaction may suppress signal transducers and activators of transcription 1 (STAT1) translocation and subsequently competitively inhibit nuclear import of IFN-stimulated gene factor 3 (ISGF3) complex. Our biochemical, structural and cellular analyses provide novel insights to pB318L that acts as an essential GGPPS that promotes viral replication and as a nuclear import protein that may be involved in immune evasion of ASFV.

INTRODUCTION

African swine fever virus (ASFV) is a giant DNA virus with a diameter of more than 200 nm and the sole member of the *Asfarviridae* family (Alonso et al., 2018). ASFV infects domestic and wild pigs and is highly contagious. ASFV infection causes fever and often lethal disease of swine and raise great threats to swine industry (Sánchez-Cordón et al., 2018; Dixon et al., 2019). Currently, no effective vaccine or other useful treatment are available against ASFV infection. The ASFV virion possesses a multi-layered structure, which from inside to outside contains the inner nucleoid, core shell, inner envelope, capsid and outer envelope (Wang et al., 2019). The inner nucleoid of ASFV is largely the ~170–190 kbp double-stranded DNA genome, which encodes more than 150 proteins involved in various stages of the viral life cycle (Dixon et al., 2013).

* Corresponding authors.
E-mail addresses: zhangheng@ihep.ac.cn (H. Zhang), dongyh@ihep.ac.cn (Y.-H. Dong).
[1] Hai-Fan Zhao, Ying Wang, and Xiao-Hong Liu contributed equally to this work.

https://doi.org/10.1016/j.virs.2025.03.013
Received 24 July 2024; Accepted 27 March 2025
Available online 2 April 2025

The initialization of ASFV DNA synthesis occurs in the swine cell nucleus (Ballester et al., 2011). The replication and virion assembly are then completed in the cytoplasm, in which the virus genome DNA lesions may be induced by production of reactive oxygen species (ROS) in macrophages.

Isoprenoids (also known as terpenes or terpenoids) are the largest and most diverse group of natural products, and more than 80,000 identified members have been characterized to date (Christianson, 2017). They are widely distributed eukaryotes (especially plants), bacteria and archaea, with diverse in structure and biological functions (Wallrapp et al., 2013; Chang et al., 2021). Productions of isoprenoids are catalyzed by a group of enzymes known as prenyltransferases (PTs). The PTs can be classified into three main types: (1) isoprenyl pyrophosphate synthase (IPPS) that catalyze the condensation of isopentenyl diphosphate (C5; IPP) with

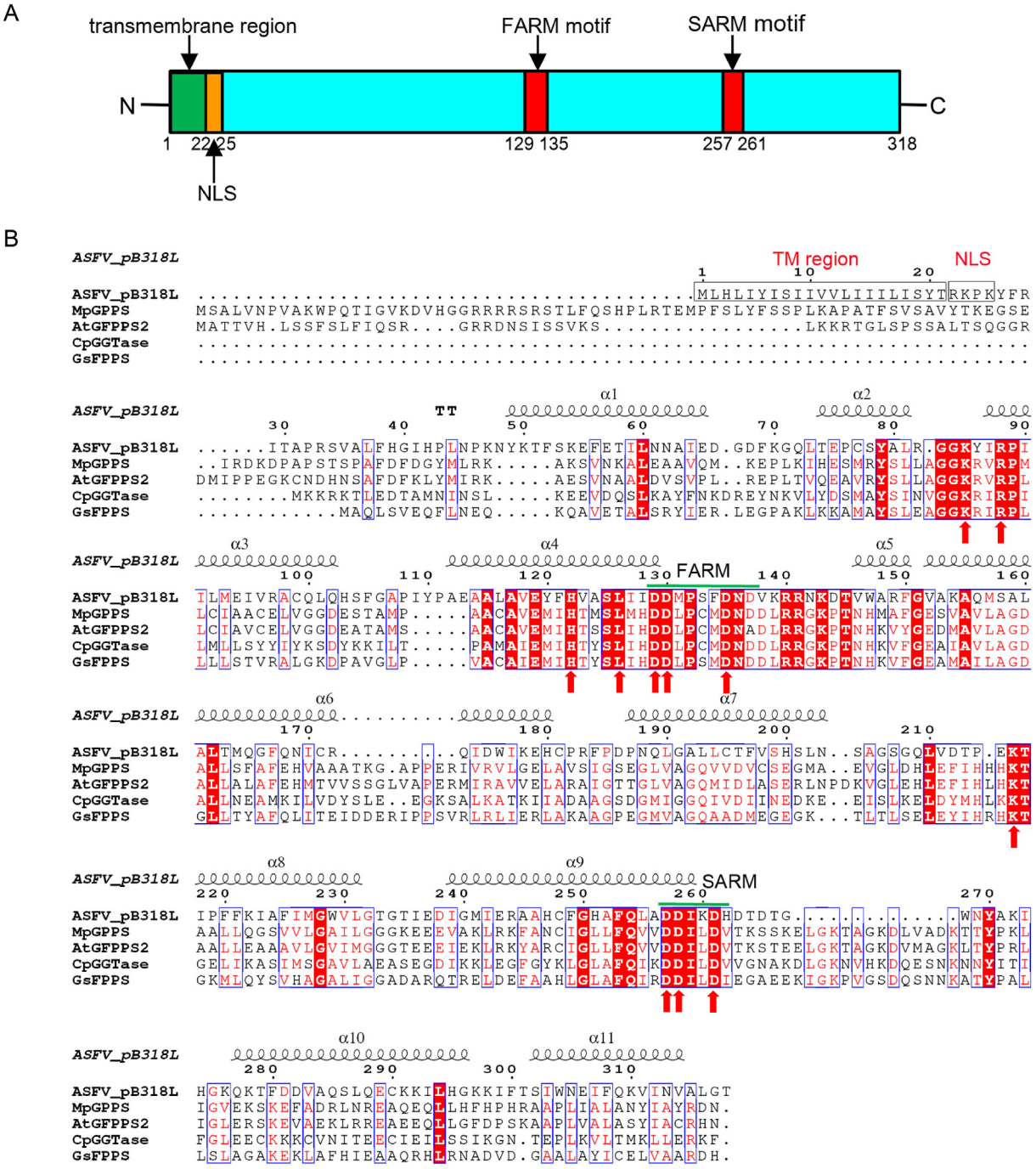

Fig. 1. The domain and sequence characteristic of ASFV pB318L. **A** Domain/motif organization of pB318L full-length protein (cyan) with annotated conserved motifs. The N-terminal transmembrane (TM) region, nuclear localization signal (NLS), FARM/SARM motifs are highlighted in green, orange and red, respectively. **B** Structure-based sequence alignment of pB318L with its representative homologs from different species performed using clustal X (version 1.81) and ESPript 3. They include ASFV pB318L (Q65164, 318 aa), *Mentha piperita* geranyl pyrophosphate synthase (MpGPPS, Q9SBR3, 377 aa), *Arabidopsis thaliana* GFPPS2 (AtGPPS, Q9LUD9, 360 aa), *Clostridium perfringens* geranylgeranyltransferase (CpGGTase, Q8XJE0, 301 aa) and *Geobacillus stearothermophilus* farnesyl pyrophosphate synthase (GsFPPS, Q08291, 297 aa). The accession number in UniProt database and the length of each sequence are labeled in the brackets. The conserved residues are boxed in blue. Identical conserved and low conserved residues are highlighted in red background and red letters, respectively. The FARM and SARM motifs are labeled using green bars. The residues used for mutagenesis study and geranylgeranyl pyrophosphate (GGPP) production assay are highlighted using red arrows.

allylic diphosphates to produce linear polymers with defined chain lengths, such as farnesyl diphosphate synthase (FPPS) and geranylgeranyl diphosphate synthase (GGPPS); (2) PTs that catalyze the cyclization of isopentenyl pyrophosphate (IPP); (3) protein PTs that catalyze the prenylation modification of a protein or a peptide by covalent addition of farnesyl pyrophosphate (C15; FPP) or geranylgeranyl pyrophosphate (C20; GGPP) (Liang et al., 2002). The previous study showed pB318L is a *trans*-PT that catalyzes the head-to-tail condensation of IPP with different allylic diphosphates, such as dimethylallyl pyrophosphate (C5; DMAPP), geranyl pyrophosphate (C10; GPP), FPP and GGPP (Alejo et al., 1997, 1999). The predominant product of pB318L-catalyzed reaction was GGPP using IPP and FPP as substrates, while prenyl diphosphates with longer chain (C30–C50) were also synthesized. pB318L harbors two conserved aspartate-rich motifs, DDx2-4D (the first aspartate rich motif, FARM, where x is any amino acid) and DDxxD (the second aspartate-rich motif, SARM) (Fig. 1A), which are characteristic of FPPSs, GGPPSs and other PTs. The pB318L is localized in the cytoplasmic viral assembly sites in ASFV-infected cells, which is associated with precursor viral membranes derived from the endoplasmic reticulum (ER) (Alejo et al., 1999). Also, the protein is localized in ER in the cells infected with the recombinant Sindbis virus carrying the complete *B318L* gene. It was supposed to act as a protein PT for the modification of some viral proteins (such as L83R), but there is no experimental evidence to verify such function till now. Recently we found pB318L can reduce the expression of type I interferon (IFN–I) and IFN-stimulated genes (ISGs) (Liu et al., 2024). Mechanically, the protein may partially affect viral pathogenicity by negatively regulating host cGAS-STING and JAK-STAT signaling pathways.

ASFV pB318L is an important protein for viral replication and harbors a putative N-terminal transmembrane (TM) region that is anchored into membrane (Alejo et al., 1997). It remains associated with precursor viral membranes derived from the endoplasmic reticulum at the viral assembly sites. As the only known virus-origin PT, these properties made it is distinct from those known PTs from other species that are located in the cytosolic. In this work, we biochemically characterized pB318L by performing structure-based mutagenesis studies. We found that pB318L structure is significantly similar to FPPS and GGPPS from plants and bacteria rather than the protein PTs. The key residues involved in its GGPP synthase activity are identified by determining their *in vitro* enzymatic activities. We also identified a unique N-terminus nuclear localization signal (NLS) that is required for nuclear import of pB318L and explored its role in pB318L function in evading the host innate immunity.

RESULTS

Structural comparison of pB318L with its homologs

We recently solved pB318L structure (PDB ID: 8HDL) lacking N-terminal 30 residues (ΔN30) including putative TM region (Fig. 1A), and performed a preliminary structural analysis (Zhao et al., 2023). The substrate-binding pocket is located between the helices α4 and α9, which harbors the conserved Asp-rich motifs FARM (residues 129–135) and SARM (residues 257–261), respectively (Fig. 1B).

A DALI search (http://ekhidna.biocenter.helsinki.fi/dali_server) revealed significant similarities between pB318L and many FPPS/GGPPS

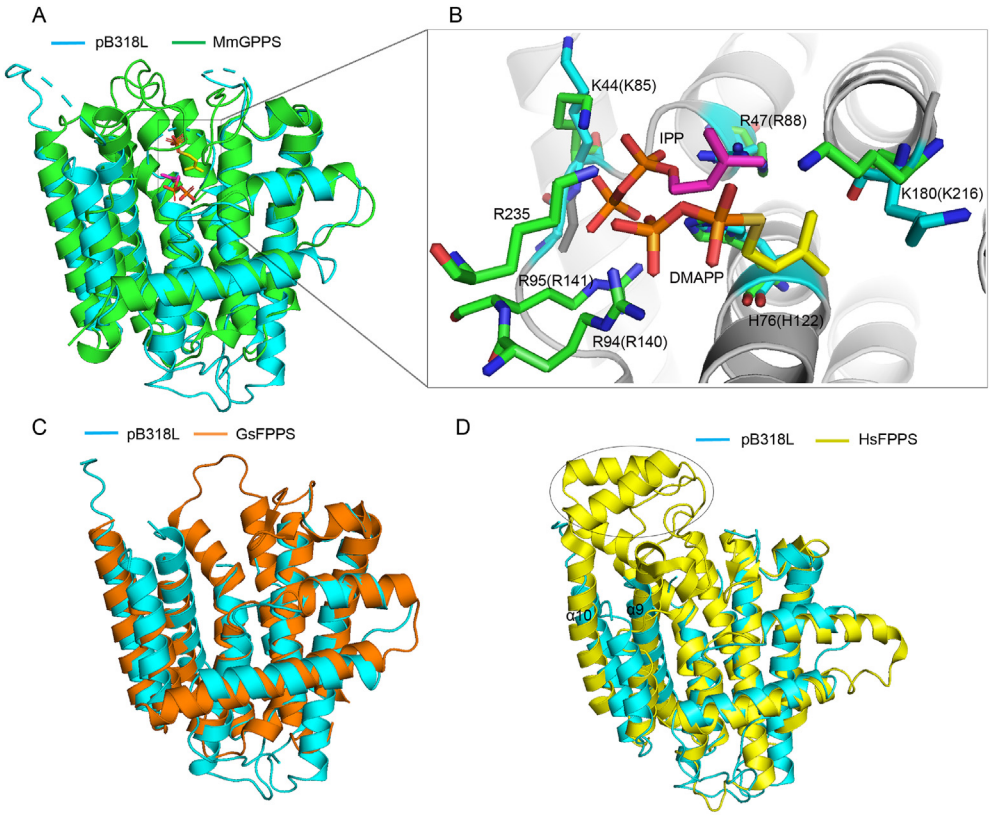

Fig. 2. Structural comparison of ASFV pB318L with its homologs from different species. **A** Structural superposition of pB318L (cyan) with the large subunit of *M. piperita* GPPS (MpGPPS, green)-isopentenyl pyrophosphate (IPP)-DMASPP complex (PDB ID: 3KRF). The IPP and DMAPP in MpGPPS are shown as magenta and yellow sticks, respectively. DMASPP (dimethylallyl thiopyrophosphate) is a DMAPP analog. **B** Close-view of the active sites of the above two proteins. The residues in brackets in pB318L correspond to those in MpGPPS. **C** Structural superposition of pB318L (cyan) with *G. stearothermophilus* FPPS (GsFPPS, PDB ID: 5AYP, orange). **D** Structural superposition of pB318L (cyan) with *Homo sapiens* FPPS (HsFPPS, PDB ID: 2F8Z, yellow). The major difference is the insertion of several helices between α9 and α10 (numbered based on pB318L) in HsFPPS structure.

from plants, bacteria and archaea (with Z-scores of 22.4–23.1) despite low amino acid sequence identities (21%–27%). Structural superposition of pB318L with the large subunit of geranyl pyrophosphate synthase (GPPS) from *Mentha piperita* (PDB ID: 3KRF) and the FPPS from *Geobacillus stearothermophilus* (PDB ID: 5AYP) showed that they exhibit very similar overall folds, with a r.m.s.d. of 1.4–1.5 Å (Fig. 2A and C). Meanwhile, structural superposition of pB318L with the FPPS from *Homo sapiens* (PDB ID: 2F8Z, with the identical sequence to that from *Sus scrofa*) reveals a moderate similarity (with a r.m.s.d. of 2.3 Å) (Fig. 2D). The major difference is the insertion of several helices between α9 and α10 (numbered based on pB318L) in *Homo sapiens* FPPS (HsFPPS) structure. Structure-based sequence alignment of pB318L with the representative homologs from plants and bacteria showed they have conserved Asp-rich motifs FARM and SARM (Fig. 1B). Meanwhile, structural comparison of pB318L with the protein PTs showed their structures are distinct (Supplementary Fig. S1). For example, the substrate peptide binding pocket of the protein PT is obviously absent in pB318L.

ASFV pB318L-IPP-DMAPP model

Considering the high structural similarity between pB318L and the GPPS from *Mentha piperita* (referred as MpGPPS, Fig. 2A), structural superposition of pB318L with MpGPPS-IPP-DMASPP (DMAPP analog) complex (PDB ID: 3KRF) (Chang et al., 2010), was performed to explore the allylic diphosphates-binding characteristic features of pB318L. The IPP and DMASPP molecules from MpGPPS can be docked into the active-site cavity of pB318L with predominantly positive charges without steric clash (Fig. 2B). The docked DMASPP showed generally favorable direct interactions with several conserved residues in pB318L. The IPP-binding residues in MpGPPS, Lys44, Arg47, His76, Arg94 and Arg95, correspond to Lys85, Arg88, His122, Arg140 and Arg141 in pB318L, respectively (Arg140 and Arg141 are missing in pB318L structure). The DMAPP-binding residue Lys180 in MpGPPS correspond to Lys216 in pB318L while Lys235 doesn't have corresponding residue in pB318L. All of the interacting-residues are highly conserved in pB318L and the

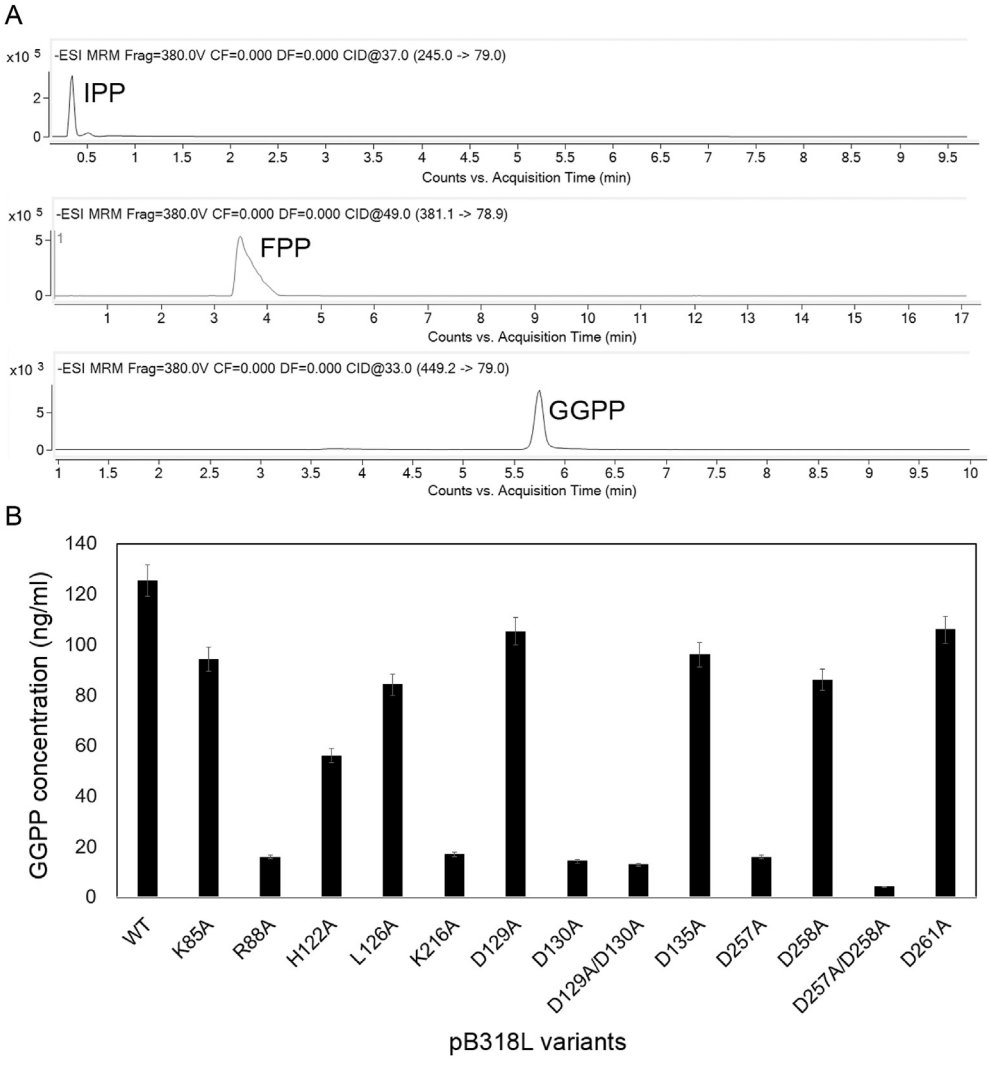

Fig. 3. Identification of the key residues for the geranylgeranyl pyrophosphate synthase (GGPPS) activity of ASFV pB318L. **A** The liquid chromatography-electrospray ionization-tandem mass spectrometry (LC-ESI-MS/MS) analysis of GGPP production catalyzed by pB318L. The total ion chromatography (TIC) of lipid ions was recorded in the negative ion detection mode. The multiple reactions monitoring mode (MRM) of LC-ESI-MS/MS was used to quantify GGPP contents in the reaction extracts. **B** GGPP production of pB318L WT and mutants. Data are presented as the mean ± standard error of the mean from three independent experiments. The GGPP production was measured at an IPP/farnesyl pyrophosphate (FPP) concentration of 100 μM.

FPPS/GPPS homologs (Fig. 1B), indicating that they may have similar substrate-binding characteristics.

Identification of key residues for GGPPS activity of pB318L

These potential IPP/DMAPP-binding residues, together with the conserved Asp residues of FARM/SARM motifs were mutated to alanines to explore their roles in substrate recognition and catalysis by determining their *in vitro* GGPP synthase activities (Fig. 3A). The previous thin layer chromatogram (TLC) analysis showed GGPP is the predominant product of pB318L-catalyzed reaction using IPP and FPP as the substrates (Alejo et al., 1997, 1999). Therefore, the enzymatic activity of pB318L was defined as its GGPP-production capacity within certain time in this study. The multiple reactions monitoring mode (MRM) of liquid chromatography-electrospray ionization–tandem mass spectrometry (LC-ESI-MS/MS) was used to quantitatively determine the GGPP contents within 60 min. The GGPP amounts catalyzed by pB318L wild-type (WT) and a series of mutants were compared under the same experimental conditions. The results showed that all mutants exhibit reduced activities compared with the wild-type (Fig. 3B). Of note, mutation of IPP-binding Arg88 and DMAPP-binding Lys216 to alanine (R88A and K216A) resulted in severe loss of GGPPS activities, to ~12% and ~15% of the WT, respectively. On the other hand, single or double mutations of catalytic FARM/SARM motifs showed Asp130 and Asp257 are essential residues for the GGPPS synthase activity (GGPP amounts were reduced to ~5% and ~12% of the WT, respectively), while mutations of the other residues (Asp129, Asp135, Asp258 and Asp261) didn't remarkably inhibit the activities.

Phylogenetic analysis of pB318L

The phylogenetic tree was constructed from the amino acid sequences of representative PTs from various species (Fig. 4). In our tree, the FPPS/GGPPS from *Brassicaceae* plants (*Arabidopsis thaliana*, *Mentha piperita* and *Oryza sativa*) and bacteria (*Geobacillus stearothermophilus*, *Clostridium perfringens* and *Shigella flexneri*), formed a branch, respectively. ASFV pB318L showed the lowest genetic distance (*P*) with the plant branch (*P* = 0.12), in which the GGPPS11 from *A. thaliana* is also one of its structural homologs with the highest similarities (Wang et al., 2016).

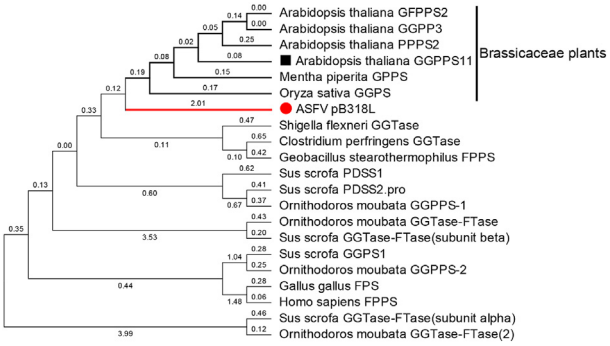

Fig. 4. The phylogenetic analysis of ASFV pB318L. All the protein sequences were downloaded from the UniProt database (their IDs are labeled in the brackets). A maximum likelihood tree was constructed using MEGA6 software (Tamura et al., 2013).They include ASFV pB318L (Q65164), *Ornithodoros moubata* GGPPS-1 (A0A1Z5KV60)/GGPPS-2 (A0A1Z5L6G0), *Sus scrofa* PDSS1 (A0A287B4S1)/PDSS2 (D0G786), *Sus scrofa* GGPS1 (A0A287ARC4), *Homo sapiens* FPPS (P14324), *Gallus gallus* FPS (P08836), *Mentha piperita* GPPS (Q9SBR3), *Arabidopsis thaliana* PPPS2 (Q9LJY2)/GFPPS2 (Q9LUD9)/GGPPS3 (Q9LUD9)/GGPPS11(P34802), *Oryza sativa* GGPS (A0A0E0ALV9), *Geobacillus stearothermophilus* FPPS (Q08291), *Clostridium perfringens* GGTase (Q8XJE0), *Shigella flexneri* GGTase (A0A0H2UXE9), *Sus scrofa* geranylgeranyltransferase-farnesyltransferase (GGTase-FTase) subunit alpha (A0A4X1UDX6) and subunit beta (A0A4X1UCT8), *Ornithodoros moubata* GGTase-FTase subunit alpha (A0A4X1UDX6) and subunit beta (A0A1Z5KX75).

Meanwhile, the genetic distance between pB318L and the IPPS from the natural hosts of ASFV, such as the decaprenyl diphosphate synthase (PDSS)1/PDSS2 from *Sus scrofa* and GGPPS-1/GGPPS-2 from *Ornithodoros moubata*, is remarkably higher than that of *Brassicaceae* plants. Moreover, pB318L also distinctly separate from the protein PTs (geranylgeranyltransferase/farnesyltransferase, GGTase/FTase) from *S. scrofa* and *O. moubata,* indicating they have distinct functions. These results suggest that ASFV pB318L may share a common ancestor with the GGPPSs from *Brassicaceae* plants, and have arisen from distinct routes of molecular evolution from the GGPPSs of its natural hosts.

Generation of pB318L full-length dimer structure by AlphaFold2

The structure of pB318L full-length (FL) monomer was predicted using the program AlphaFold2 (https://alphafold.ebi.ac.uk) (Fig. 5A). The GGPPS domain (residues 31–318) had a high confidence (pLDDT score 93.3) and was very similar to the crystal structure (with the r.m.s.d. of ~0.4 Å). On the other hand, the N-terminal region (residues 1–30) showed a moderate confidence (pLDDT score 72.5) probably because of lacking homologous structures. The two predicted monomers were then superposed into pB318L dimer crystal structure to generate the FL dimer structure.

The N-terminal transmembrane (TM) region (residues 1–21, in green) is folded into a stable helix and stretches out for potential membrane-binding (Fig. 5A). The two TM helices resemble the pincers of a crab to be simultaneously anchored into the membrane. In the downstream of the N-terminal TM region, there is a motif (residues 22-RKPK-25) that is rich in positive residues (Fig. 1A and B). The motif was predicted to be a putative nuclear localization signal (NLS, motif PAT4:22-rKKPK-25) using PSORT II tool. The putative NLS (in red) is present as a flexible loop and is also exposed to the solvent for potential interactions with the nuclear transporters [such as karyopherin subunit alpha 1 (KPNA1), discussed below].

Subcellular localization of ASFV pB318L in nucleus and cytoplasm

To determine the subcellular localization of pB318L in cells, HeLa cells were transfected with pHA-B318L expressing the hemagglutinin (HA)-tagged pB318L in the pCAGGS vector and analyzed by laser confocal microscopy. Considering the HA tag may be affected by the N-terminal TM region, the tag was placed in the C-terminus of pB318L. Staining of HeLa cells with an anti-HA antibody showed that pB318L was distributed in both the nucleus and the cytoplasm while the latter accounts for the majority (Fig. 5B), consistent with the results obtained using anti-pB318L antibody (data not shown). Meanwhile, the immunofluorescence results indicated that pB318L ΔNLS (deletion of the putative NLS) was mainly distributed in the extra-nuclear region instead of nucleus (Fig. 5B). Taken together, these results confirmed the NLS is involved in the nuclear localization of pB318L.

The subcellular localization of pB318L in the cytoplasm was evaluated in HeLa cells by co-transfecting pB318L-HA-expressing plasmid and various sub-organelle markers plasmids. After 24 h of transfection, the immunofluorescence analysis was performed to determine the subcellular distribution of pB318L protein. The results showed that pB318L was co-localized with multiple protein markers (Fig. 5C), including Sec61β (endoplasmic reticulum marker), Tomm20 (mitochondrial marker), Rab5 (early endosome marker), Rab7 (late endosome marker), as well as CD63 (exosome marker). Collectively, these results indicate that pB318L is widely distributed in the cytoplasm, including the endoplasmic reticulum, mitochondria, early endosomes and late endosomes. Of note, the co-localization of Tomm20 and Sec61β suggesting pB318L can target the mitochondria outer membrane and endoplasmic reticulum membrane, which is probably mediated by its N-terminal TM region.

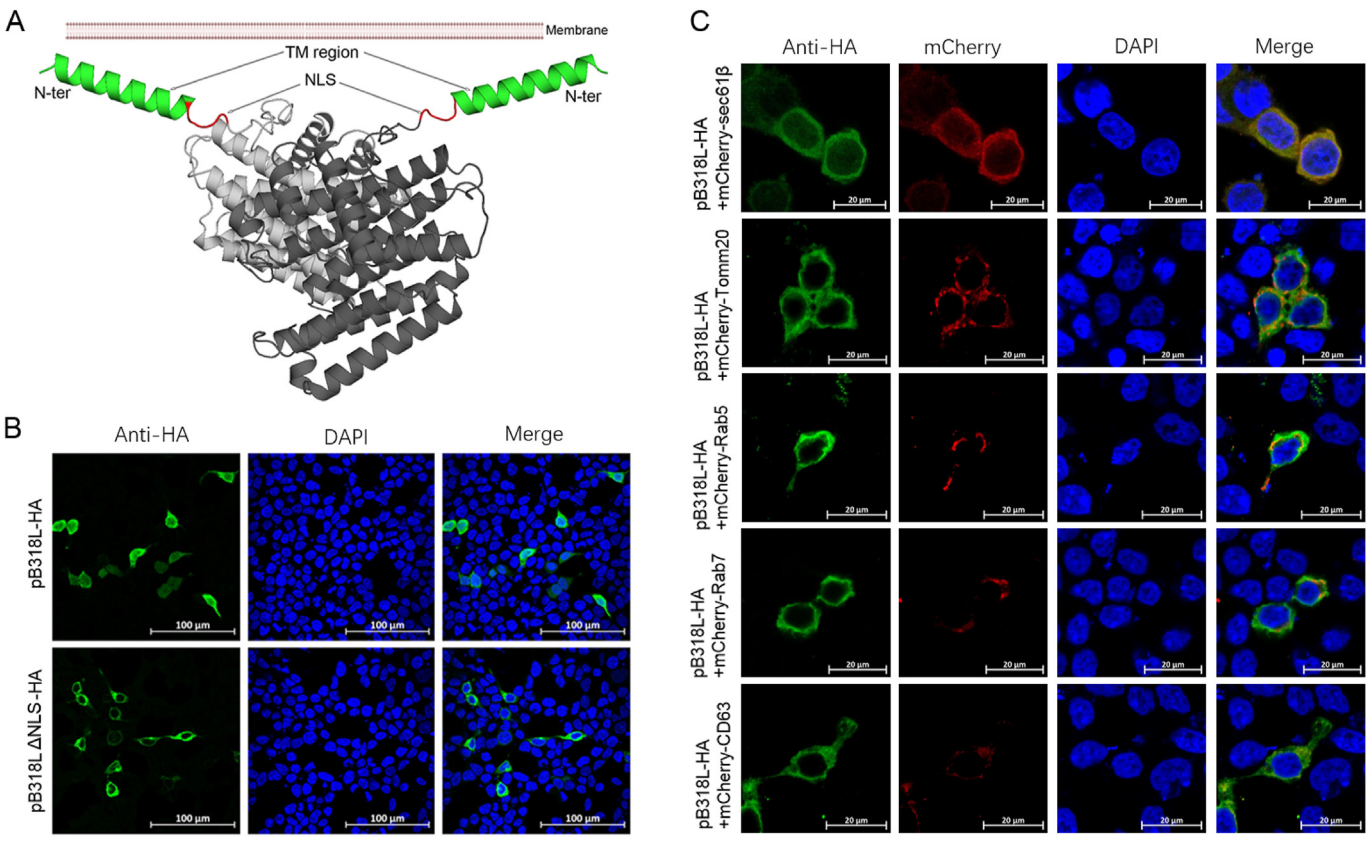

Fig. 5. Subcellular localization analysis of pB318L. **A** ASFV pB318L full-length (FL) dimer structure predicted by AlphaFold2. The transmembrane (TM) region and nuclear localization signal (NLS) are highlighted in green and red, respectively. **B** Subcellular distribution of full length pB318L protein and its ΔNLS in nucleus. FITC-labeled pB318L and DAPI stained nucleus were shown in its original color green and blue. **C** Subcellular distribution of pB318L full-length protein in cytoplasm. Fluorescence microscopy of HeLa cells co-transfected with plasmids pB318L-HA and mCherry-SEC61β, mCherry-TOMM20, mCherry-Rab5, mCherry-Rab7 and mCherry-CD63, respectively. FITC-labeled proteins and mCherry fusion proteins were shown in its original color green and red, respectively, and the merged image was presented in yellow signal. The nucleus was stained with DAPI for visualization.

The NLS is required for the suppression of STAT1 translocation by binding to KPNA1

To explore whether pB318L is involved in the activation of IFN-β signaling through the nuclear localization, HEK-293T cells were transfected with pB318L expression plasmids, interferon stimulated response element (ISRE) luciferase reporter plasmid (pISRE-Luc) and internal reference plasmid. The luciferase assay results showed that the IFN-β promoter was significantly inhibited by ectopically expressed pB318L (Fig. 6A). The results indicated that pB318L is involved in the regulation of type I interferon signal transduction. To investigate the regulation of pB318L on the nuclear translocation of IFN-stimulated gene factor 3 complex [ISGF3, composed of signal transducers and activators of transcription 1, signal transducers and activators of transcription 2 (STAT1, STAT2) and IRF9], we tested the effect of pB318L expression on the location of endogenous STAT1 and IRF9. The results showed that STAT1 and IRF9 localize in the nucleus upon IFN-β treatment, and localized in the cytoplasm during co-existing with pB318L (Fig. 6B and C). The co-IP results also showed that pB318L co-immunoprecipitated with STAT1 (Fig. 6D). On the other hand, deletion of the NLS (ΔNLS) disrupted the location of STAT1 and IRF9 in the cytoplasm. The results suggested that pB318L may inhibit the nuclear translocation of ISGF3 complex to inhibit IFN-β signaling by its NLS.

It is known that the nuclear translocation of ISGF3 complex is mediated by the interaction between STAT1 and nuclear transporter KPNA1 (karyopherin subunit alpha 1). In order to explore whether pB318L interferes with the normal nuclear import of ISGF3 complex by interacting with KPNA1, we co-transfected pB318L with KPNA1. The results showed that pB318L and KPNA1 are co-located in the nucleus, as well as their co-immunoprecipitation revealed by Co-IP (Fig. 6E and F). However, pB318L ΔNLS was located in the cytoplasm instead of the nucleus when co-transformed with KPNA1, indicating the NLS plays an essential role in KPNA1-binding (Fig. 6F). Our findings indicate that the unique NLS is responsible for pB318L to antagonize JAK-STAT signaling pathway by hijacking KPNA1. The nuclear translocation of ISGF3 complex is therefore inhibited and the expression of downstream ISGs is decreased.

DISCUSSION

ASFV pB318L is the only known IPPS from virus, which is important for viral replication (Alejo et al., 1997, 1999). Therefore, it is interesting to explore its possible origin and molecular evolution process. In this study, structural analysis suggest that pB318L is significantly similar to FPPS and GGPPS from plants and bacteria rather than those from its natural hosts (*S. scrofa* and *O. moubata*). Meanwhile, the remarkable structural difference between pB318L and protein GGTase/FTase, indicating it cannot function as a GGTase or FTase, which catalyzes the attachment of a farnesyl lipid group to the cysteine residue located in the C-terminal tetrapeptide. The phylogenetic analysis further indicated the evolution route of ASFV pB318L may arise from ancestral long-chain GGPPS from brassicaceae plants (although their amino acid sequence identities are only ~25%). On the other hand, phylogenetic analysis suggests that pB318L have arisen from distinct routes of molecular evolution from FPPS/GGPPS from its natural hosts. Similarly, a previous phyletic patterns and phylogenetic analysis suggest that the

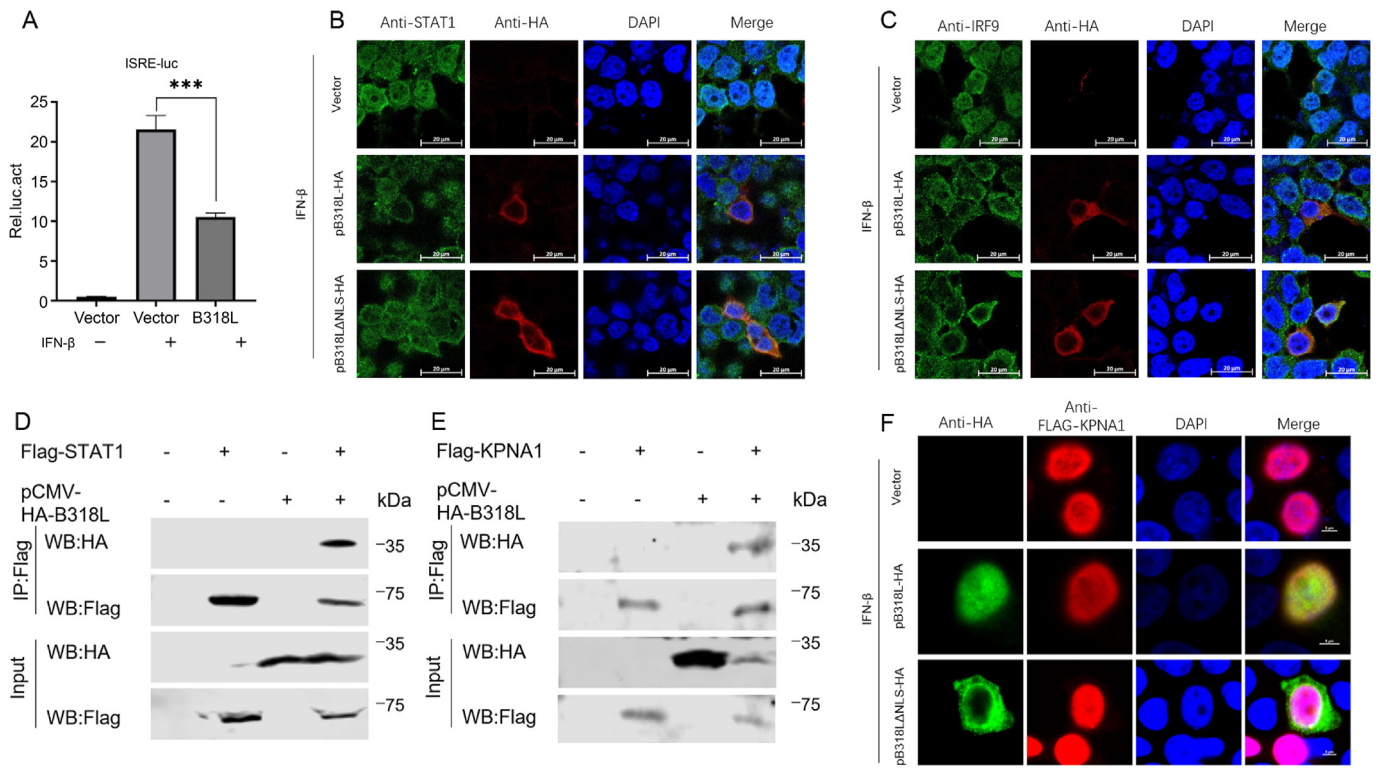

Fig. 6. pB318L negatively regulates the IFN-β signaling pathway by inhibiting signal transducers and activators of transcription 1 (STAT1) nuclear translocation. **A** Luciferase assay indicated the negative effects of pB318L overexpression on interferon stimulated response element (ISRE). Graphs data are shown as means ± SD; n = 3. ***, $P < 0.01$, Rel.luc.act, relative luciferase activity. **B, C** Colocalization of pB318L with endogenous STAT1 or IRF9. HeLa cells were transfected with empty vector or pB318L-HA or pB318LΔNLS-HA, after 24h treated with IFN-β (1000 U/mL) for another 4 h. STAT1 and IRF9 antibodies were used to label the endogenous expression of STAT1 and IRF9 proteins. The localization of pB318L, STAT1 and IRF9 were observed through confocal microscopy. **D, E** Co-IP analysis of the interaction between pB318L and STAT1/karyopherin subunit alpha 1 (KPNA1). HEK293T cells were transfected with a plasmid expressing pB318L-HA (the HA tag is located in the C-terminus of pB318L), along with a plasmid expressing Flag-tagged STAT1 or KPNA1, respectively. At 24 h post-transfection (hpt), Co-IP was performed to detect the interaction between pB318L and STAT1/KPNA1. **F** Colocalization of pB318L with KPNA1. HeLa cells were co-transfected with pB318L-HA and FLAG-KPNA1 expression plasmid. After 24 h, the cells were treated with IFN-β (1000 U/mL) for 4 h before observation under a confocal microscope. It is noted the scale bar is 20 μm in Fig. 6B and C and 5 μm in Fig. 6F.

NAD-dependent ligase of the extant Nucleo-Cytoplasmic Large DNA Viruses (NCLDV) was most likely acquired from a bacteriophage at the early stages of evolution of eukaryotes (Yutin and Koonin, 2009). The captured distantly related or even non-homologous host genes may be beneficial for the functional complexity and fitness of dsDNA virus (Koonin and Krupovic, 2022). The information on the molecular evolution of pB318L might provide a clue to assist in understanding how pB318L emerged in the evolutional history of ASFV.

The previous study showed pB318L was localized in the endoplasmic reticulum as well as in cytoplasmic viral assembly sites that is associated with precursor viral membranes derived from the endoplasmic reticulum (Alejo et al., 1999). Our subcellular localization analysis also showed pB318L can be localized in the cytoplasm (including the endoplasmic reticulum membrane and mitochondria outer membrane), which is mediated by its N-terminal TM region. In addition to its role as electron carrier in mitochondria, coenzyme Q is distributed in nearly all cellular membranes, such as plasma membrane, endoplasmic reticulum-Golgi and lysosomes, to perform widespread cellular functions (Guerra and Pagliarini, 2023). The pB318L-producing GGPP could serve as precursors of the coenzyme Q (respiratory quinones) side chains that is produced in functional mitochondria (Alejo et al., 1997, 1999), which may provide additional energy and in turn promote the assembly, maturation and release of viral particles (Fig. 7). Alternately, these GGPP may serves as the prenyl donors for the possible prenylation modification of cellular (such as Rho GTPases) or ASFV proteins (such as pL83L and pI9R), which is required during virus replication and morphogenesis (Quetglas et al., 2012).

Several proteins from ASFV were recently found to inhibit host innate immune response by targeting the JAK-STAT pathway. For example, ASFV pH240R interacted with IFNAR1 and IFNAR2 to disrupt the interaction of IFNAR1-TYK2 and IFNAR2-JAK1. Additionally, pH240R inhibited the phosphorylation of IFNAR1, TYK2 and JAK1 induced by IFN-α, resulting in the suppression of the nuclear import of STAT1 and STAT2 and the expression of ISGs (Ye et al., 2024). Similarly, ASFV pF778R can counteract the activation of JAK-STAT pathway through inhibition of STAT1 nuclear translocation and therefore act as a negative regulator of the type I interferon signaling pathway (Chen et al., 2023). We recently found pB318L interacted with IFN receptors (IFNAR1/IFNAR2) to block the interaction of IFNAR1/TYK2 and IFNAR2/JAK1 to negatively regulate JAK-STAT signaling pathways (Liu et al., 2024). We constructed an ASFV strain with *B318L* gene expression interruption (ASFV-intB318L) and infected PAMs with ASFV-HLJ/18 and ASFV-intB318L. Upon IFN-α treatment of PAMs, ASFV-intB318L induced more ISGs and phosphorylation of STAT1/2 compared to ASFV-WT, indicating that pB318L also inhibits the JAK-STAT signaling pathway during ASFV infection. In this study, we showed pB318L can directly interact with STAT1 and nuclear transporter KPNA1. A unique N-terminal NLS following the TM region was discovered in pB318L and deletion of the NLS abolished its location in the nucleus. Deletion of the NLS disrupted pB318L interaction with KPNA1, which function as an adapter of nuclear transport receptor KPNB1 (Karyopherin β1) that transports cargos from the cytosol to nucleus. Subsequently, the hijacking of KPNA1 by pB318L may block the entry of ISGF3 complex (STAT1-STAT2-IR9) into the nucleus (Fig. 7). Therefore, pB318L can inhibit the translocation

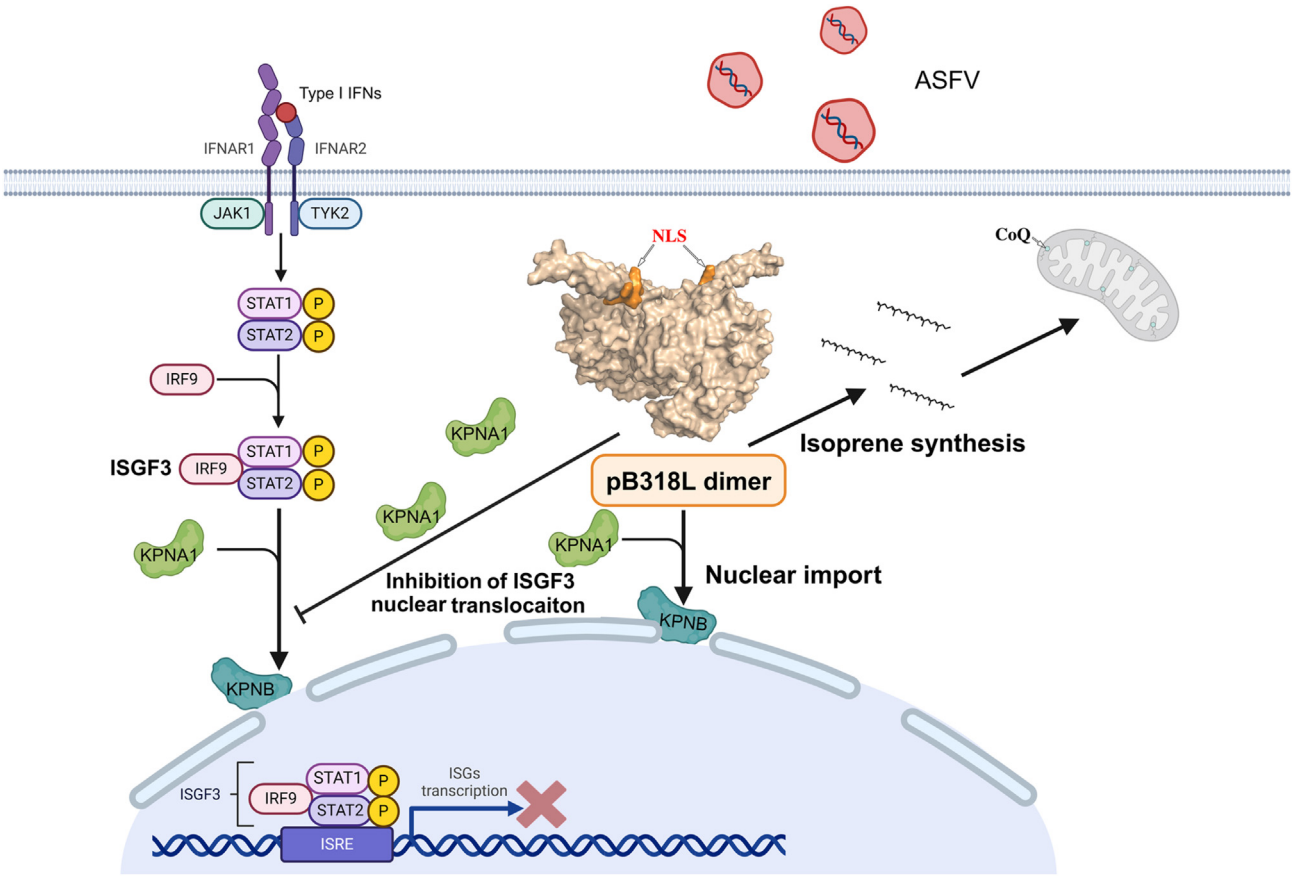

Fig. 7. A supposed mechanism on the dual role of pB318L in viral replication. pB318L can function as a typical GGPPS that produces isoprenoids [such as geranyl pyrophosphate (GPP), FPP and GGPP] that may act as the isoprenoid tail of the coenzyme Q in mitochondria. On the other hand, as a nuclear import protein harboring a unique N-terminal NLS, one of its potential functions is the inhibition of IFN-stimulated gene factor 3 (ISGF3) complex translocation to antagonize JAK-STAT signaling pathway.

of ISGF3 complex (STAT1-STAT2-IR9) to antagonize JAK-STAT signaling pathway.

Here we showed pB318L, as a membrane-binding protein, can be imported into nucleus, although the intact function in the nucleus remains unknown. Several viral and eukaryotic membrane-binding proteins have been found to be located in the nucleus to perform their multiple functions (Švančarová and Betáková, 2018; Arzt et al., 2004; Park et al., 2008; Liu et al., 2018). For example, the membrane-binding region of influenza virus M1 protein mediates its location in the cytoplasmic membrane or the virus envelope, while its NLS mainly mediates M1 entry from the cytoplasm into the nucleus to interact with viral RNA or ribonucleoprotein complexes in the nucleus (Švančarová and Betáková, 2018). Also, Gp110 protein of Epstein–Barr virus (EBV) contains a signal peptide that can localize in both the nuclear membrane and the ER membrane (Park et al., 2008). It is noted the observations that pB318L localization in the nucleus, as well as its interaction with KPNA1 and STAT1, were obtained using the pB318L-expressing plasmid in which the HA tag was placed in the C-terminus of the protein in this study. Our recent study showed pB318L was solely localized in the cytoplasm when the HA tag was placed in the N-terminus of pB318L in the recombinant plasmid (Liu et al., 2024). Consistently, we confirmed pB318L was only localized in the cytoplasm and found the protein didn't show the interaction with STAT1 or KPNA1 using the above plasmid with N-terminal HA tag (Supplementary Fig. S2 and Fig. S3). Therefore, we supposed the N-terminal HA tag, which is neighboring the TM region and NLS, may disrupt the NLS binding by KPNA1/STAT1 and affect the translocation of pB318L in the nucleus.

The previous site-directed mutagenesis studies on the IPPSs indicated that all the Asp residues in the FARM/SARM motifs are important for catalysis, except the last one in SARM motif (Marrero et al., 1992; Joly and Edwards, 1993; Song and Poulter, 1994; Koyama et al., 1996). For example, mutations of the three Asp in FARM as well as first and second Asp in SARM to Ala in yeast FPPS, decreased k_{cat} by 10^4–10^5, whereas mutation of the third Asp in SARM decreased k_{cat} only by ~10^2 (Song and Poulter, 1994). Our structure-based mutagenesis study and GGPP production assay revealed Asp130 (the second Asp in FARM motif) and Asp257 (the first Asp in SARM motif) are critical residues for enzymatic activity, while the other Asp residues are probably dispensable. On the hand, we tested the effects of the two mutations (D130A and D257A) on IFN-β-induced ISRE promoter activity and found that they did not affect the inhibitory effect of pB318L on ISRE (Supplementary Fig. S4). The results indicated that the enzyme activity of pB318L did not affect its inhibitory effect on the JAK-STAT signaling pathway.

Our recent study found pB318L can inhibit ISGs production whereas D129A mutant (the first Asp in FARM motif) did not inhibit IFN-I and ISGs expression (Liu et al., 2024). Here, the GGPPS activity assays showed the GGPP-production capacity of D129A mutant was not significantly decreased, suggesting it is not a key residue involved the enzymatic activity. In this case, the inhibition of type IFNs and ISGs production by pB318L is likely independent on its GGPPS activity. Moreover, our enzymatic assay showed the IPP-binding residue Arg88 and DMAPP-binding residue Lys216 are key residues for the GGPPS activity, which are located in the active center of pB318L structure. On the other hand, the five residues located upstream from the FARM, have been shown to be involved

in product chain-length determination, in which the aromatic residues (such as phenylalanine or tyrosine) may interferes with the chain elongation of the final product (Wallrapp et al., 2013; Chang et al., 2021). Notably, sequence analysis showed the fifth and sixth residue located upstream from the FARM is an alanine (Ala124) and a serine (Ser125) in pB318L, respectively (Fig. 1B). In avian FPPS, mutation of Phe112 and Phe113, corresponding to Ala124 and Ser125 in pB318L, resulted in the product specificity shifting from FPP to GGPP (F112A), GFPP (F113S) and longer products (F112A/F113S) (Tarshis et al., 1996). The presence of Ala124/Ser125 may explain the previous observation that longer chain (C30–C50) can be synthesized in pB318L-catalyzed reaction (Alejo et al., 1997, 1999), and their roles in controlling products length require further structural and biochemical studies.

CONCLUSIONS

Our structure-function study reveal the dual role of ASFV pB318L that acts a typical geranylgeranyl-diphosphate synthase and a nuclear import protein. Structure of pB318L assists in identification of the unique features and key residues for its enzymatic activity, which may facilitate the antiviral drug design. Moreover, structural comparison and phylogenetic analysis of ASFV pB318L, the only known viral GGPPS, provide a clue to assist in understanding the molecular evolution of pB318L. Taken together, our study provides novel insights into the role of ASFV pB318L interference with type I IFN signaling in evading the host innate immunity, which may useful for the vaccine development against ASFV.

MATERIALS AND METHODS

Cells, plasmids and antibodies

The DNA sequence encoding pB318L-ΔN40 (deletion of N-terminal 40 residues) was amplified by PCR from the plasmid harboring pB318L full-length sequence and cloned into the modified pET28a-SUMO (Novagen, USA) in which the cleavable ubiquitin-like-specific protease 1 (ULP1) fused with N-terminal His_6 tag was introduced. The recombinant plasmids were transformed into *E. coli* DH5α cloning strain and plated onto LB-kanamycin plates. The plasmid was isolated and transformed into an *E. coli* BL21 (DE3) star expression strain (Invitrogen). Site-directed mutagenesis of pB318L-ΔN40 was performed by a PCR-based technique according to the QuikChange site-directed mutagenesis strategy (Stratagene) following the manufacturer's instructions. The mutant genes were sequenced and found to only contain the desired mutations.

HEK293T cells and HeLa cells were grown in DMEM (Gibco) supplemented with 1% Penicillin-Streptomycin (Gibco) and 10% FBS (Gibco). The full-length DNA sequence encoding pB318L was cloned into pcDNA3.1 fused with C-terminal HA tag. Plasmids encoding porcine STAT1 (GenBank No: NM_213769.1), STAT2 (GenBank No: HM462244.1), IRF9 (GenBank No: NM_001078670.1) and KPNA1 (GenBank No: NM_001163405.1) were constructed by cloning the synthesized sequences into pcDNA3.1 with Flag tags fused to the end. All constructed plasmids were confirmed through sequencing.

The plasmids encoding mCherry-SEC61β, mCherry-TOMM20, mCherry-Rab5, mCherry-Rab7 and mCherry-CD63, were purchased from Addgene. Monoclonal rabbit anti-HA and mouse anti-Flag were purchased from Beyotime Biotechnology. Alexa Fluor 488-conjugated goat anti-rabbit IgG (H + L) and Alexa Fluor 594-conjugated goat anti-mouse IgG (H + L) Abs were purchased from Proteintech Group. Anti-STAT1 Rabbit mAb (14,994)and IRF-9 Rabbit mAb (76,684) were purchased from Cell Signaling Technology.

Protein expression and purification

Bacterial cells expressing pB318L-ΔN40 were grown to mid-log phase in LB media at 37 °C in the presence of 50 μg/mL kanamycin. Induction of protein expression was initiated by adding isopropyl-1-thio-β-D-galactopyranoside (IPTG) to the culture to a final concentration of 0.4 mM, and the cells were grown at 16 °C. Cells were pelleted after 20 h by centrifugation at 6000*g* for 10 min at 4 °C. The cell pellet was resuspended in a buffer containing 20 mM Tris (pH 8.0), 300 mM NaCl, 2 mM β-mercaptoethanol and 1 mM PMSF, and lysed by ultrasonication on ice. The soluble N-terminally His-SUMO-tagged pB318L-ΔN40 was purified by affinity chromatography with nickel-nitrilotriacetic acid resin (Bio-Rad, USA) and the tag was removed by protease ULPI overnight hydrolysis and reloaded with 20 mM imidazole. EMCV 2C-ΔN was further purified by gel filtration (Superdex 75, GE Healthcare, USA) equilibrated in a buffer containing 20 mM Tris (pH 8.0), 300 mM NaCl and 2 mM DTT using an ÄKTA Purifier System (GE Healthcare, USA). Highly purified protein fractions were pooled and concentrated. Protein concentrations were determined using the Bio-Rad protein assay kit. All pB318L-ΔN40 variants were expressed and purified following the same procedures (including the same buffers) to the wild-type protein.

GGPP production by recombinant pB318L

In vitro assays were performed in reaction solution (20 mM HEPES, pH 7.5, 5 mM $MgCl_2$, 5 μg/mL of BSA). The reaction mixtures (100 μL) include 100 μM IPP, 100 μM FPP and 500 ng purified pB318L-ΔN40 (WT and mutants) and were incubated for 1 h at 37 °C. Then the reaction mixtures were mixed with methanol (100 μL) and vortexed for 5 min. The samples were centrifuged at 12,000 × *g* for 15 min at 4 °C and the supernatant was detected as described below.

Quantitative determination of GGPP by LC-MS

The ultra-high-performance liquid chromatography-triple quadrupole-tandem mass spectrometry (UHPLC-QQQ-MS/MS) systems (Ma et al., 2023), was used to quantitatively determined GGPP contents from the reactions catalyzed by pB318L-ΔN40.

The system is composed of an Agilent 1290 Infinity LC pump and a 6490 triple quadrupole mass spectrometer. An Agilent ZORBAX Extend C18 column (50 mm × 2.1 mm, 1.8 μm) was used for separation, and the column temperature was maintained at 35 °C. Solvent A was 0.05% aqueous ammonium acetate, and solvent B was 100% acetonitrile. The chromatograph program was as follows at a flow of 0.30 mL/min: 0–1.0 min, 2% solvent B; 1.0–5.0 min, linear gradient to 30% B; 5.0–5.5 min, linear gradient to 50% B; 5.5–7.5 min, linear gradient to 100% B; 7.5–11.0 min, maintained at 100% B, 11.0–11.1 min, linear gradient to 2% B, and 11.1 min–15 min, maintained 2% B. Negative mode analysis was performed in multiple reaction monitoring (MRM) mode. The MS/MS ion transitions monitored and MS parameters were optimized with IPP/FPP/GGPP standards. The ion source parameters were set as follows: drying gas temperature 200 °C (nitrogen), drying gas flow 16 L/min, nebulizer 30 p.s.i., sheath gas heater 350 °C, sheath gas flow 12 L/min, and capillary voltage 3.5 kV (ESI-). The concentrations of IPP, FPP and GGPP were calculated using the corresponding standard curves.

Phylogenetic analysis of ASFV pB318L

All the protein sequences were downloaded from the UniProt database. Multiple sequence alignments were carried out using ClustalW of the Megalign program (DNAStar software). A maximum likelihood tree was constructed using MEGA6 software (Tamura et al., 2013). The reliability of the generated trees was determined with 1000 replicates of the data set.

Transfection and dual-luciferase reporter assays

HEK293T cells were grown in a 24-well plate and cotransfected with 100 ng of IFN-β-luc and 500 ng of pB318L-HA, or 500 ng of the empty vector using Lipofectamine 3000 Transfection Reagent (Invitrogen) following the instructions provided by the manufacturer. At 24 h post-

transfection, the cells were stimulated with IFN-β and then lysed using Luciferase Cell Culture Lysis Reagent (Yeasen Biotechnology). Luciferase activity (LA) was measured using Tecan Spark 10 M Multimode Plate Reader (Switzerland) with the dual-luciferase reporter assay system (Yeasen Biotechnology), following the instructions from the manufacturer. The relative LA was calculated by normalizing to the Renilla LA.

Confocal microscopy and co-localization analysis

HeLa cells were transfected with expressing plasmids using Lipofectamine 3000 Transfection Reagent (Invitrogen). At 24 h after transfection, the cells were fixed with 4% paraformaldehyde for 10 min at room temperature and permeabilized with 0.1% Triton X-100 for 15 min. After washing three times with PBS-T, the cells were incubated in the dark with goat anti-mouse IgG H&L (Alexa Fluor 594) and goat anti-rabbit IgG H&L (Alexa Fluor 488) at 37 °C for 1 h. This was followed by nuclear staining with 4, 6-diamidino- 2-phenylindole (DAPI). The samples were detected using a Nikon Instruments Inc. confocal system.

Co-immunoprecipitation (Co-IP) and immunoblot analysis

Co-IP and immunoblot analysis were performed as recently described (Liu et al., 2024). In brief, for Co-IP, the cells were collected and lysed in lysis buffer (50 mM Tris-HCl, pH 7.4, 150 mM NaCl, 5 mM MgCl2, 1 mM EDTA, 1% Tris-HCl, and 10% glycerol) containing 1 mM PMSF and 1 × protease inhibitor cocktail (Basel, Switzerland, Roche). Then, cell lysates were incubated with anti-flag (M2) beads (Sigma-Aldrich, St. Louis, MO, USA) or added indicated antibodies and protein A + G Plus-Agarose (Santa Cruz Biotechnology, Dallas, TX, USA). After incubation 4–8 h at 4 °C, the beads were washed three times with lysis buffer. For immunoblot analysis, the samples were separated by 10%–12% sodium sulfate polyacrylamide gel electrophoresis (SDS-PAGE) and then transferred to a polyvinyl difluoride (PVDF) membrane (Sigma-Aldrich, St. Louis, MO, USA). After incubation with primary and secondary antibodies, the membrane is visualized by the Odyssey Dual Color Infrared Fluorescence Imaging System (LI-COR, Lincoln, NE, USA).

STATISTICS AND REPRODUCIBILITY

Differences between the control group and the experimental groups were analyzed using GraphPad 5.0 software by two-way analysis of variance (ANOVA) using the least-square difference multiple-comparison test. Differences were considered statistically significant at $P < 0.001$ was considered highly significant. The results are presented as the mean ± the standard deviation (SD).

DATA AVAILABILITY

All the data generated during the current study are included in the manuscript.

ETHICS STATEMENT

This article does not contain any studies with human or animal subjects performed by any of the authors.

AUTHOR CONTRIBUTIONS

Hai-Fan Zhao, Ying Wang and Xiao-Hong Liu: investigation, data curation, formal analysis and writing-original draft. Xian-Hui Liu, Zhi Geng and Zeng-Qiang Gao: formal analysis and investigation; Li Huang, Chang-Jiang Weng, Yu-Hui Dong and Heng Zhang: conceptualization, data curation, formal analysis, supervision, writing-original draft, writing-review and editing, funding acquisition. All the authors read and approved the manuscript.

CONFLICT OF INTEREST

The authors declare no conflict of interest. The funders had no role in study design, data collection and analysis, decision to publish, or preparation of the manuscript.

ACKNOWLEDGEMENTS

We thank Dr. Fengxia Zhang (Institute of Genetics and Developmental Biology, Chinese Academy of Sciences) for providing technical support on GGPP determination by LC-QQQ-MS/MS. This study was financially supported by the grants from the National Natural Science Foundation of China to Heng Zhang (31970152), the Strategic Priority Research Program of CAS to Yu-Hui Dong (XDB37040302) and the CAS Emergency Research Project on African Swine Fever to Yu-Hui Dong (Grant KJZD-SW-L06-01).

APPENDIX A. SUPPLEMENTARY DATA

Supplementary data to this article can be found online at https://doi.org/10.1016/j.virs.2025.03.013.

REFERENCES

Alejo, A., Andrés, G., Viñuela, E., Salas, M.L., 1999. The African swine fever virus prenyltransferase is an integral membrane trans-geranylgeranyl-diphosphate synthase. J. Biol. Chem. 274, 18033–18039.
Alejo, A., Yáñez, R.J., Rodríguez, J.M., Viñuela, E., Salas, M.L., 1997. African swine fever virus trans-prenyltransferase. J. Biol. Chem. 272, 9417–9423.
Alonso, C., Borca, M., Dixon, L., Revilla, Y., Rodriguez, F., Escribano, J.M., Consortium, I.R., 2018. ICTV virus taxonomy profile: Asfarviridae. J. Gen. Virol. 99, 613–614.
Arzt, S., Petit, I., Burmeister, W.P., Ruigrok, R.W., Baudin, F., 2004. Structure of a knockout mutant of influenza virus M1 protein that has altered activities in membrane binding, oligomerisation and binding to NEP (NS2). Virus Res. 99, 115–119.
Ballester, M., Rodríguez, C.C., Pérez, M., Gallardo, C., Rodríguez, J., Salas, M., Rodriguez, F., 2011. Disruption of nuclear organization during the initial phase of African swine fever virus infection. J. Gen. Virol. 85, 8263–8269.
Chang, H.Y., Cheng, T.H., Wang, A.H.-J., 2021. Structure, catalysis, and inhibition mechanism of prenyltransferase. IUBMB Life 73, 40–63.
Chang, T.H., Hsieh, F., Ko, T., Teng, K., Liang, P., Wang, A.H., 2010. Structure of a heterotetrameric geranyl pyrophosphate synthase from mint (*Mentha piperita*) reveals intersubunit regulation. Plant Cell 22, 454–467.
Chen, Q.C., Li, L., Liu, L.J., Liu, Z.K., Guo, S.B., Tan, C., Chen, H.C., Wang, X.R., 2023. African swine fever virus pF778R attenuates type I interferon response by impeding STAT1 nuclear translocation. Virus Res. 335, 199190.
Christianson, D.W., 2017. Structural and chemical biology of terpenoid cyclases. Chem. Rev. 117, 11570–11648.
Dixon, L., Sun, H., Roberts, H., 2019. African swine fever. Antivir. Res. 165, 34–41.
Dixon, L.K., Chapman, D.A.G., Netherton, C.L., Upton, C., 2013. African swine fever virus replication and genomics. Virus Res. 173, 3–14.
Guerra, R.M., Pagliarini, D.J., 2023. Coenzyme Q biochemistry and biosynthesis. Trends Biochem. Sci. 48, 463–476.
Joly, A., Edwards, P.A., 1993. Effect of site-directed mutagenesis of conserved aspartate and arginine residues upon farnesyl diphosphate synthase activity. J. Biol. Chem. 268, 26983–26989.
Koonin, E.V., Krupovic, M., 2022. A life LINE for large viruses. ELife 11, e83488.
Koyama, T., Tajima, M., Sano, H., Doi, T., Koike-Takeshita, A., Obata, S., Nishino, T., Ogura, K., 1996. Identification of significant residues in the substrate binding site of *bacillus stearothermophilus* farnesyl diphosphate synthase. Biochemistry 35, 9533–9538.
Liang, P.H., Ko, T., Wang, A.H., 2002. Structure, mechanism and function of prenyltransferases. Eur. J. Biochem. 269, 3339–3354.
Liu, H., Zhang, H., Wu, X., Ma, D., Wu, J., Wang, L., Jiang, Y., Fei, Y., Zhu, C., Tan, R., et al., 2018. Nuclear cGAS suppresses DNA repair and promotes tumorigenesis. Nature 563, 131–136.
Liu, X., Chen, H., Ye, G., Liu, H., Feng, C., Chen, W., Hu, L., Zhou, Q., Zhang, Z., Li, J., et al., 2024. African swine fever virus pB318L, a trans-geranylgeranyl-diphosphate synthase, negatively regulates cGAS-STING and IFNAR-JAK-STAT signaling pathways. PLoS Pathog. 20, e1012136.

Ma, Y., Chen, Q., Wang, Y., Zhang, F., Wang, C., Wang, G., 2023. Heteromerization of short-chain trans-prenyltransferase controls precursor allocation within a plastidial terpenoid network. J. Integr. Plant Biol. 65, 1170–1182.
Marrero, P.F., Poulter, D., Edwards, P.A., 1992. Effects of site-directed mutagenesis of the highly conserved aspartate residues in domain II of farnesyl diphosphate synthase activity. J. Biol. Chem. 267, 21873–21878.
Park, S.J., Seo, M.D., Lee, S.K., Lee, B.J., 2008. Membrane binding properties of EBV gp110 C-terminal domain; evidences for structural transition in the membrane environment. Virology 379, 181–190.
Quetglas, J.I., Hernáez, B., Galindo, I., Muñoz-Moreno, R., Cuesta-Geijo, M., Alonso, C., 2012. Small rho GTPases and cholesterol biosynthetic pathway intermediates in African swine fever virus infection. J. Gen. Virol. 86, 1758–1767.
Sánchez-Cordón, P.J., Montoya, M., Reis, A.L., Dixon, L.K., 2018. African swine fever: a re-emerging viral disease threatening the global pig industry. Vet. J. 233, 41–48.
Song, L., Poulter, C.D., 1994. Yeast farnesyl-diphosphate synthase: site-directed mutagenesis of residues in highly conserved prenyltransferase domains I and II. Proc. Natl. Acad. Sci. U. S. A 91, 3044–3048.
Švančarová, P., Betáková, T., 2018. Conserved methionine 165 of matrix protein contributes to the nuclear import and is essential for influenza A virus replication. Virol. J. 15, 187.
Tamura, K., Stecher, G., Peterson, D., Filipski, A., Kumar, S., 2013. MEGA6: molecular evolutionary genetics analysis version 6.0. Mol. Biol. Evol. 30, 2725–2729.
Tarshis, L.C., Proteau, P.J., Kellogg, B.A., Sacchettini, J.C., Poulter, C.D., 1996. Regulation of product chain length by isoprenyl diphosphate synthases. Proc. Natl. Acad. Sci. U. S. A 93, 15018–15023.
Wallrapp, F.H., Pan, J., Ramamoorthy, G., Almonacid, D.E., Hillerich, B.S., Seidel, R., Patskovsky, Y., Babbitt, P.C., Almo, S.C., Jacobson, M.P., et al., 2013. Prediction of function for the polyprenyl transferase subgroup in the isoprenoid synthase superfamily. Proc. Natl. Acad. Sci. U. S. A 110, E1196–E1202.
Wang, C., Chen, Q., Fan, D., Li, J., Wang, G., Zhang, P., 2016. Structural analyses of short-chain prenyltransferases identify an evolutionarily conserved GFPPS clade in brassicaceae plants. Mol. Plant 9, 195–204.
Wang, N., Zhao, D., Wang, J., Zhang, Y., Wang, M., Gao, Y., Li, F., Wang, J., Bu, Z., Rao, Z., et al., 2019. Architecture of African swine fever virus and implications for viral assembly. Science 366, 640–644.
Ye, G., Zhang, Z., Liu, X., Liu, H., Chen, W., Feng, C., Li, J., Zhou, Q., Zhao, D., Zhang, S., et al., 2024. African swine fever virus pH240R enhances viral replication via inhibition of the type I IFN signaling pathway. J. Gen. Virol. 98, e0183423.
Yutin, N., Koonin, E.V., 2009. Evolution of DNA ligases of nucleo-cytoplasmic large DNA viruses of eukaryotes: a case of hidden complexity. Biol. Direct 4, 51.
Zhao, H., Zhang, H., She, Z., Gao, Z., Wang, Q., Geng, Z., Dong, Y., 2023. Exploring AlphaFold2's performance on predicting amino acid side-chain conformations and its utility in crystal structure determination of B318L protein. Int. J. Mol. Sci. 24, 2740.